Spectropolarimetry of 3CR 68.1: A Highly Inclined Quasar[1]

M. S. Brotherton
Institute of Geophysics and Planetary Physics, Lawrence Livermore National Laboratory, 7000 East Avenue, P.O. Box 808, L413, Livermore, CA 94550; mbrother@igpp.llnl.gov

Beverley J. Wills
McDonald Observatory and Astronomy Department, University of Texas, Austin, TX 78712; bev@astro.as.utexas.edu

Arjun Dey[2]
KPNO/NOAO[3], 950 N. Cherry Avenue, P.O. Box 26732, Tuscon, AZ 85726

Wil van Breugel
Institute of Geophysics and Planetary Physics, Lawrence Livermore National Laboratory, 7000 East Avenue, P.O. Box 808, L413, Livermore, CA 94550; wil@igpp.llnl.gov

Robert Antonucci
Physics Department, University of California at Santa Barbara, Santa Barbara, CA 93106; ski@ginger.physics.ucsb.edu

ABSTRACT

We present Keck spectropolarimetry of the highly polarized radio-loud quasar 3CR 68.1 ($z = 1.228, V = 19$). The polarization increases from 5% in the red (4000Å rest-frame) to >10% in the blue (1900Å rest-frame). The broad emission lines are polarized the *same* as the continuum, which shows that 3CR 68.1 is not a blazar as it has sometimes been regarded in the past. We also present measurements of the emission lines and a strong, blueshifted, associated absorption line system, as well as a detection at the emission-line redshift of Ca II K absorption, presumably from stars in the host galaxy.

3CR 68.1 belongs to an observationally rare class of highly polarized quasars that are neither blazars nor partially-obscured radio-quiet QSOs. Taking into account 3CR 68.1's other unusual properties, such as its extremely red spectral energy distribution and its extreme lobe dominance, we explain our spectropolarimetric results in terms of unified models. We argue that we have a dusty, highly inclined view of 3CR 68.1, with reddened scattered (polarized) quasar light diluted by even more dust-reddened quasar light reaching us directly from the nucleus.

Subject headings: line: profiles — quasars: emission lines — quasars: general — quasars: absorption lines — galaxies: individual: 3CR 68.1 — techniques:polarimetric

[1]Based on observations at the W. M. Keck Observatory.

[2]Currently at Johns Hopkins University, dey@skysrv.pha.jhu.edu.

[3]The National Optical Astronomy Observatories are operated by the Association of Universities for Research in Astronomy under cooperative agreement with the National Science Foundation.

1. Introduction

3CR 68.1 ($z = 1.228, V = 19$) is a quasar with a unique combination of extreme properties. The optical-UV continuum is among the reddest of any known quasar, with $F_\nu \propto \nu^{-6}$ in the UV (Boksenberg, Carswell, & Oke 1976; Smith & Spinrad 1980). 3CR 68.1 is one of the most highly polarized quasars, with a polarization in a broad bandpass from 3000-8000Å of 7.5% ± 1.3% at 52° ± 5° (Moore & Stockman 1981, 1984). The lobes of 3CR 68.1 mark the quasar as a powerful radio source, but the extremely faint radio core (≈ 1 mJy at 5 GHz, Bridle et al. 1994) makes this object one of the most lobe-dominant quasars. Under Unified Schemes, it is the most highly inclined 3CR quasar known (e.g., Orr & Browne 1982; Hoekstra, Barthel & Hes 1997). Extreme objects like 3CR 68.1 may provide clues as to how their properties may be related in less extreme AGNs.

3CR 68.1 has been classified as a blazar because of its high polarization and red color (e.g., Ledden & Odell 1985), but we thought this was unlikely because the degree of polarization and position angle did not change between measurements made 6 months apart (Moore & Stockman 1981, 1984), and the optical continuum level is not violently variable (Smith & Spinrad 1980). Also, it does not have the core-dominant radio structure always characteristic of radio-selected blazars. In fact, in the revised 3C sample (Laing, Riley, & Longair 1983; Hoekstra et al. 1997), it is the most lobe-dominant quasar with the largest projected lobe separation, large even among radio galaxies, suggesting a radio axis close to the sky plane.

Most highly polarized QSOs (HPQs) can be classified as radio-quiet (including many BAL QSOs), or as radio-loud blazars. The polarization mechanism in radio-quiet QSOs is scattering (e.g., BAL QSOs: Hines & Wills 1995; Goodrich & Miller 1995; Cohen et al. 1995; Miller 1997; Ogle 1997; Schmidt et al. 1997; Brotherton et al. 1997; and IRAS non-BAL QSOs: Wills & Hines 1997; Wills et al. 1992), perhaps with a geometry similar to that found in polarized Seyfert 2 galaxies like NGC 1068 (e.g., Miller & Antonucci 1985, and the review by Antonucci 1993). In addition, many highly polarized, low-ionization BAL QSOs and IRAS QSOs appear reddened compared with UV-selected QSOs (Sprayberry & Foltz 1992).

Do non-blazar radio-loud HPQs exist? OI 287 appears to be one – a lobe-dominant radio-loud quasar, optically quiescent with a constant optical polarization of ≈8% aligned parallel to the extended radio structure (Antonucci & Ulvestad 1988; Rudy & Schmidt 1988). The broad emission lines and continuum show similar degrees of polarization but the narrow emission lines are unpolarized (Goodrich & Miller 1988). Apparently OI 287 is a normal quasar seen only in scattered light because a thin, dusty disk obscures the central regions (Rudy & Schmidt 1988; Goodrich & Miller 1988; Antonucci, Kinney, & Hurt 1993). Certainly there are buried quasars in which broad lines and continuum are revealed only in scattered (polarized) light (e.g., Cygnus A, 3C 324, 3C 265, IRAS 09104+4109). Some of these are called radio galaxies.

We hypothesized that the polarization mechanism in 3CR 68.1 is not optical synchrotron as in blazars, but rather scattering with dust absorption reddening the UV-optical spectrum. We therefore obtained spectropolarimetry of 3CR 68.1 with Keck II in order to test this hypothesis and determine the polarization mechanism.

Furthermore, as part of the complete 3CR sample, whose selection is predominantly based on isotropic extended radio emission, an understanding of 3CR 68.1 can address the question of the prevalence of red quasars that might escape detection by usual optical selection criteria (e.g., Webster et al. 1995).

§ 2 describes our observations and data reduction procedure. § 3 presents our results and shows that the polarization increases dramatically to shorter wavelengths, that the broad emission lines are polarized

at the same level as the continuum. We also discuss the absorption spectrum and our spectroscopic detection of the host galaxy of 3CR 68.1. § 4 argues that scattering by dust or electrons is indeed the polarization mechanism, and that both the direct and scattered light are reddened. We show several models for the spectrum of 3CR 68.1, exploring the ranges in reddening, scattered light fraction, and host galaxy contribution. We briefly discuss how 3CR 68.1 fits into unification schemes. § 5 is a summary.

2. Observations and Data

On 1996 December 10 (UT), we observed 3CR 68.1 with the Low Resolution Imaging Spectrometer (Oke et al. 1995) in spectropolarimetry mode (Goodrich, Cohen, & Putney 1995; Cohen et al. 1997) on the 10 m Keck II telescope. The 300 line mm^{-1} grating blazed at 5000Å with a $1''$ slit (at 226°, approximately the parallactic angle) gave an effective resolution $\leq$ 10Å (FWHM of comparison lamp lines); the dispersion was 2.5Å $pixel^{-1}$. The seeing just prior to the observation was $1\farcs1$. The observation was broken into four 15 minute exposures, one for each waveplate position (0°, 45°, 22.5°, 67.5°). We observed a bright star through UV and IR polaroid filters to measure and calibrate the wavelength-dependent polarization position angle changes imparted by the instrument optics. The polarization measurement efficiency was essentially 1.0 at all wavelengths. We observed the flux standard Feige 110 (at the parallactic angle, seeing $1.3''$) both in direct light and with an OG 570 filter. No order-blocking filter was used for the 3CR 68.1 observation because of its weak blue flux and the decreased second-order efficiency of the grating. Then we observed the polarized standard star HD245310 (at the parallactic angle; Schmidt, Elston, & Lupie 1992) in all four waveplate positions in order to determine the zero point of the polarization position angle.

We reduced our data to one-dimensional spectra using standard techniques within the IRAF NOAO package. The rms uncertanties in the dispersion solution were 0.2Å, and we used sky lines to ensure that our zero point was accurate to 0.1Å. Wavelengths are air wavelengths. We followed standard procedures (Miller, Robinson, & Goodrich 1988; Cohen et al. 1997) for calculating Stokes parameters and uncertanties. We used the measurements of Massey et al. (1988) and Massey & Gronwall (1990) for flux calibration.

The Galactic absorption in the direction of 3CR 68.1 is small, $A_V = 0.15$ (Burstein & Heiles 1982). We give observed quantities below, but where noted we have corrected our data for the Galactic extinction using the curve of Cardelli et al. (1989).

3. Results

Figure 1 shows our main results, including the total flux-density spectrum (F_λ), the percentage polarization (P), the electric vector polarization position angle (θ), and the polarized flux-density ($\frac{P}{100} \times F_\lambda$). Except for the total flux spectrum, the data are binned (100Å in the continuum, but more finely around the emission lines as described below). The bins were first formed using the one-dimensional raw-count spectra from each waveplate position; the error bars assume Poisson noise from the object and background sky counts, plus the CCD read noise. These binned data then determine the binned linear Stokes parameters, including P and θ, with errors propagated through the polarization calculation.

Figure 2 shows details of several spectral regions in total light, including C III] λ1909, Mg II λ2800, and the narrow lines and Ca II K absorption feature at the red end of the spectrum.

3.1. Polarimetry

The continuum polarization increases toward shorter wavelengths, from ≈5% at the red end of our spectrum to >10% at the blue end. Within the uncertanties θ is constant across the entire range, with an average $\approx 53.3^\circ \pm 0.2^\circ$. The high polarization and position angle are consistent with the broadband results of Moore & Stockman (1984), suggesting that the polarization has not varied over more than a decade.

Open squares in Fig. 1 designate finer bins coincident with some of the more prominent spectral features (observed wavelength range of the bins): C III] λ1909 (4140-4220Å and 4260-4360Å for the broad wings, 4220-4260Å for the narrower core), [Ne IV] λ2424 (5385-5415Å), Mg II λ2800 (6040-6170Å and 6270-6440Å for the broad wings, 6170-6200Å and 6240-6270Å for the narrower core emission, and 6200-6240Å for the absorption doublet), [O II] λ3727 (8290-8325Å), and [Ne III] λ3869 (8605-8635Å). The Mg II and C III] lines appear polarized at similar levels and position angles as the continuum. The strong forbidden lines, [O II] λ3727 and [Ne III] λ3869 appear unpolarized in the polarized-flux spectrum, although the uncertanties are too large to be sure.

3.2. Emission-Line Spectrum

Table 1 gives parameters for the emission lines in the total flux spectrum of 3CR 68.1. The uncertanties are based on choosing extreme, but still reasonable, high and low continua, thus representing the range in probable values.

In both C III] λ1909 and Mg II λ2800 there are clear inflections suggesting "narrow" and "broad" components. In addition to total line measurements, we fitted Gaussians to these separate components (making a simple linear interpolation across the absorption in the Mg II profile–certainly an underestimate for the associated Mg II absorber). Again, uncertanties represent the range in measurements for reasonable continuum choices.

We derive $z_{em} = 1.228$, which is in agreement with that from the broad lines, by averaging values for several narrow lines. This is the same value as obtained by Smith & Spinrad (1980).

3.3. Absorption-Line Spectrum

Table 2 gives measurements of the wavelengths and equivalent widths for absorption lines in the total flux spectrum of 3CR 68.1. We identify a number of low-ionization associated absorption lines at $z_{abs} = 1.2258$, and a Ca II K feature at $z_{abs} = 1.2287$ (Ca II H is coincident with the [Ne III] λ3967 line). The measurements of the Mg II absorption are more uncertain than suggested by the table because of the narrow Mg II emission component. The absorption lines are labeled in the upper panel of Figure 1.

Our results differ from those of Aldcroft et al. (1994) in several respects. Their spectrum is of higher resolution (350 km s^{-1}), but lower signal-to-noise ratio. We find a lower blueshift for the Mg II doublet (≈300 km s^{-1} instead of 2000 km s^{-1}), which seems robust in light of our low uncertanties and good agreement among lines, both in emission and absorption (the Fe II absorbers, too weak for Aldcroft et al. to have found, have redshifts that match that of Mg II and Mg I). The absolute agreement in wavelength between our results and Aldroft et al. is good (about 100 km s^{-1}); the cause of the blueshift difference is our adopted z_{em}; we use $z_{em} = 1.228$, while Aldcroft et al. use the less accurate $z_{em} = 1.240$. We do

not see the intervening Mg II absorber at $z = 0.7750$ that they report. We do not separate the absorption feature at 7093.5Å into a doublet even though our resolution should be sufficient to do so, therefore we do not support Aldcroft et al.'s identification of Na I at $z = 0.2021$. We tentatively identify the line with He I λ3187, although this line is not commonly seen in absorption.

Relative to the Mg II absorption, the Ca II K feature is strong and seems unlikely to be entirely interstellar. Its redshift is larger than that of the other absorption lines, and is consistent with z_{em} for the narrow emission lines, which suggests an origin in the stars of the host galaxy of 3CR 68.1. Comparing the equivalent width of this feature with the feature in the elliptical galaxy template of Kinney et al. (1996) would suggest that at 3900Å rest-frame, one quarter of the total flux in 3CR 68.1 is contributed by the host galaxy (see also § 4).

4. Discussion

4.1. The Spectral Energy Distribution

3CR 68.1 would not be found in an UV-excess survey. Some 10% of quasars in the 3CR sample, 3CR 68.1 being the most extreme, are significantly redder than bright optically selected quasars (Smith & Spinrad 1980). 3CR 68.1 has been observed in many wavebands. Figure 3 shows the spectral energy distribution (SED) of 3CR 68.1, from the far IR through the 2 keV X-rays, using measurements from the literature as noted in the caption. 3C 110, a normal 'blue' lobe-dominated quasar, is also shown for comparison.

The UV continuum is so weak that Bregman et al. (1985) argue that the large ratio of low-ionization to high-ionization line intensities is the result of photoionization by a separate soft X-ray component, giving rise to an extended partially ionized zone where strong low-ionization lines can be produced. A simpler explanation is that the quasar continuum and line spectrum are highly reddened, and emission-line clouds see a less obscured ionizing continuum than does an observer. The lack of a 2200Å dust absorption feature is not a strong argument against reddening: no 2200Å feature is seen in the Small Magellanic Cloud (SMC) reddening 'law' (Prevot et al. 1984); even for Galactic dust, the 2200Å feature can be filled in by scattering, in geometries possible for 3CR 68.1 (e.g., Witt, Thronson, & Capuano 1992). A 2200Å dust feature is also absent in the spectra of BAL QSOs (Sprayberry & Foltz 1992; Hines & Wills 1995). Also, the composition of extragalactic dust may differ from that found in the Milky Way.

Figure 4 compares our total flux spectrum with the photometry of Neugebauer et al. (1979) and Smith & Spinrad (1980). There is good agreement at blue wavelengths, and a (≈20%) difference at red wavelengths. Given the uncertanties in the flux calibration and our narrow slit, the general agreement is satisfactory. It seems probable that 3CR 68.1 has not varied significantly during the last twenty years.

4.2. The Polarization Mechanism

The polarization mechanism in 3CR 68.1 is probably scattering by a non-spherical distribution of either small dust grains or electrons. Other mechanisms can be ruled out:

1. Polarized synchrotron radiation: This mechanism fails to account for the broad-emission lines polarized the same as the continuum.

2. Galactic interstellar polarization: The interstellar polarization toward two stars close to the line of sight, SAO 55659 and SAO 55667 (<1° from 3CR 68.1), is ≤0.4% (D. Wills, private communication).

3. Host Galaxy interstellar polarization: The observed polarization shape and maximum differ significantly from a Serkowski Law, and as we show below, the maximum polarization is significantly greater than $9\times E(B-V)$, the polarization observed toward aligned dust-reddened lines of sight in the Milky Way.

Scattering by electrons or small dust grains ($2\pi a/\lambda << 1$) can result in very high polarization (§ 4.3) that is essentially wavelength independent. Large grains, which polarize light with a stronger wavelength dependence, scatter less efficiently.

We propose that the polarized spectrum arises from scattering of central quasar light, and that the rise in polarization to shorter wavelengths results from dilution by a redder spectrum. We further propose that the diluting spectrum is the quasar spectrum seen directly but reddened by dust, with some possible contamination by starlight from the host galaxy. It is likely that interstellar polarization from our galaxy or the host galaxy is small, so we do not include it. Hence the total observed spectrum of 3CR 68.1 can be described:

$$Total_\lambda = S_{\lambda,A_S} + D_{\lambda,A_D} + H_\lambda + NLR, \quad (1)$$

where S_{λ,A_S} is a scattered QSO spectrum reddened by an extinction A_S, D_{λ,A_D} is the direct QSO spectrum reddened by an extinction A_D, H_λ is the host galaxy spectrum, and NLR is the spectrum of the narrow-line region which is unpolarized and is emitted probably from an extended region outside or coincident with the scattering region. The scattered spectrum is equal to the polarized spectrum divided by the polarization p_s, of the scattered light alone.

To illustrate quantitatively the plausibility of our picture, and to constrain the fraction of scattered light and reddening towards the central quasar, we have matched composite model spectra to the total-light SED of 3CR 68.1. We first adjusted our spectrum to the photometry of Neugebauer et al. (1979). Free parameters are the intrinsic polarization of the scattered light, p_s, assumed to be wavelength-independent, and the fraction of host galaxy starlight. The strength of the Ca II K absorption feature suggests up to one quarter of the total light at 3900Å rest-frame may be host galaxy starlight. We note that Palomar 5m image-tube plates show no extensions characteristic of a luminous host galaxy (Longair & Gunn 1975). We use the elliptical galaxy template of Kinney et al. (1996) to represent the starlight contribution. We represent the spectrum of the unreddened central quasar by a mean spectrum of lobe-dominated quasars (based on spectra of the HST sample described by Wills et al. 1995). The scattered light spectrum is derived from this mean spectrum by scaling and reddening it using an SMC-type extinction law (Prevot et al. 1984) with $A_V = 0.7$ to match the observed polarized flux density spectrum, then dividing by p_s. After subtracting the host galaxy starlight and scattered light from the SED, we are left with a spectrum that we fit with a reddened central quasar spectrum.

Figure 5 presents four model composite spectra. Table 3 summarizes the model parameters, along with those of two intermediate cases. Models A, B, and C include no contribution from the host galaxy, and have $p_s = 80\%$, 50%, and 20%. The direct line-of-sight reddening required is $A_V = 1.2$, 1.3, and 1.6, respectively. Models A_G, B_G, and C_G cover the same range in p_s, and include a host galaxy contribution of 25% of the total flux density at 3900Å. The deduced line-of-sight reddening is then $A_V = 1.1$, 1.2, and 1.5, respectively. Also tabulated is the ratio of scattered to direct light after correction for reddening. Our comparison in Figure 5 extends over the range in our templates, from rest-frame B to H; the fits over the

range of our Keck data are in good agreement for the continuum, but if the SED from § 4.1 is correct in the near-IR, Figure 5 shows that models without a large elliptical host galaxy contribution are preferred.

Assuming $H_o = 50$ km s^{-1} Mpc^{-1} and $q_o = 0$, and using the observed spectrum and the known Galactic reddening, the absolute rest-frame B magnitude for 3CR 68.1 is $M(B) = -26.6$. Under the parameters of model A and dereddening the total light spectrum by $A_V = 1.2$, the intrinsic unreddened $M(B) = -28.2$. This result is not very model dependent. Therefore 3CR 68.1 is one of the most optically luminous 3CR quasars, more in line with its radio luminosity, which is one of the highest among 3CR quasars. The radio and optical luminosities then follow the trend found by Wills & Brotherton (1995).

4.2.1. Other Red, Scattered Light, Radio-Loud Quasars

There are few quasars with unusual combinations of properties similar to that of 3CR 68.1. As mentioned in § 1, the quasar OI 287 (Antonucci, Kinney, & Hurt 1993; Goodrich & Miller 1988; Rudy & Schmidt 1988) has a high, stable optical polarization, a quiescent optical flux, blueshifted associated absorption, and is lobe dominant; OI 287 differs from 3CR 68.1 in that its polarization position angle is parallel to its radio axis. WN J0717+4611 (De Breuck et al. 1998) is another highly polarized red quasar, a steep spectrum radio source that is neither a blazar nor radio-quiet QSO. Its polarization is perpendicular to the radio jet axis. It has been proposed that these quasars are partially obscured, with red colors as a result of dust extinction, and polarization arising from scattering along less obscured lines of sight. 3CR 68.1 and objects such as these constitute a separate class of HPQ distinct from OVVs and radio-quiet QSOs. There are other radio-loud type 2 (NLR dominated) objects known, of quasar-like luminosities, with broad lines and continua seen in scattered light – presumably 'buried' quasars, e.g., Cygnus A (Ogle et al. 1997), 3C 324 (Cimatti et al. 1996), 3C 265 (Dey & Spinrad 1996), and IRAS 09104+4109 (Hines & Wills 1993).

4.3. Geometry and Unified Schemes

3CR 68.1 is a classic quasar, judging by its luminosity, and broad UV emission lines of typical equivalent width. At 178 MHz it is one of the three most powerful 3CR quasars in the compilation by Laing et al. (1983). The extreme dominance of the powerful lobes in 3CR 68.1, the largest projected lobe separation of any 3CR source, the reddest continuum of any quasar, and the highest scattered-light polarization of any 3CR source, immediately suggests a connection with highly inclined AGN in Unified Schemes. It is also of interest for testing Unified Schemes as it is a member of the only sample with complete optical identifications, selected by an essentially orientation-independent quantity directly related to the power of the central engine – the low frequency (178 MHz) radio flux-density.

Barthel (1989) based the arguments for the unification of radio-loud quasars and FR II radio galaxies on the 3CR sample, suggesting that radio galaxies are quasars at axial inclinations greater than the half opening angle of a geometrically and optically thick dusty torus, about 45°, so that their quasar nuclei are obscured. A variety of observational techniques have already shown that many 3CR radio galaxies harbor hidden quasar nuclei, and ionization and scattering 'cones' have been found along the radio jet direction (e.g., Tran et al. 1998). In principle the polarization and reddening properties of the 3CR sample could be used to deduce the thickness of the obscuring torus as a function of inclination. Hill, Goodrich, & DePoy (1996) partially perform this exercise by looking for broad lines in the near infrared (where dust reddening is less) for a complete sample of 11 3C radio sources (8 narrow-line radio galaxies, two broad-line radio

galaxies, plus 3C 273). They find that the majority of objects have their broad-line regions reddened by $A_V \approx 3.0$, and their narrow-line regions by $A_V \approx 1.5$. We investigate the properties of 3CR 68.1 in light of this Unification Scheme.

Figure 6 compares the observational results with the results of a simple scattering model (after Brown & McLean 1977, see also Wills et al. 1992) in which we assume a uniformly filled cone of wavelength-independent scatterers and a scattering optical depth of unity appropriate for high polarization efficiency. The geometry of the cone is defined by the inclination i of its axis to the observer's line-of-sight, and the cosine of its half-opening angle θ_c. The intrinsic polarization of light scattered towards the observer is p_s, and Scattered/Direct is the observed ratio of scattered to direct light assuming no obscuration. Grid lines of various i and $cos\theta_c$ are shown. From the position of the models of Table 3 on the grid, the cone half-opening angle is between 26° and 46°, and the inclination $i > 41°$. For an ideal 'virtual' cone with an axis along the radio jets (the central engine axis) the polarization position angle (E-vector) is perpendicular to the radio axis, but the observed position angle for 3CR 68.1 is $\approx 60°$ to the radio axis. This discrepancy suggests a partially-filled virtual cone, or clumpy obscuration within a virtual cone. In this case the cone determined from Figure 6 will be defined by the scatterers that we 'see'; it is tilted in the plane of the sky by 30°, and its opening angle is smaller than the size of the virtual cone.

The smaller inclinations consistent with the polarization of 3CR 68.1 are near the Barthel model dividing value of 45°. The modest reddening towards the center ($A_V \approx 1 - 1.5$) is also between values for radio galaxies and UV-selected quasars. It may be helpful to realize that the observed continuum is especially steep because the UV is shifted to observed wavelengths, not because the reddening is especially high. The line-of-sight would be skimming the torus in this case. However, the extreme lobe-dominance and large lobe separation are not consistent with smaller inclinations.

The larger inclinations, corresponding to jets almost in the plane of the sky, are consistent with the radio structure and the polarization results, but in this case we would expect the direct view of the center to be completely blocked by a thick torus. One way out is for the torus to be geometrically thin, a possibility also suggested for the other scattering-polarized radio-loud quasar OI 287. This might also tie in with the most luminous AGNs having the thinnest dusty disks (e.g., Antonucci et al. 1993).

The strong, blueshifted, Mg II absorption in 3CR 68.1, identified by Aldcroft et al. (1993, 1994), and confirmed here, is sufficiently deep that the absorbing gas must lie at least in the direct path, and perhaps also in the scattered light path. In Unified Schemes lobe-dominant, high-inclination quasars are more likely to show absorption along the line-of-sight (for 3C quasars – Wills et al. 1995, see also Aldcroft et al. 1993). 3CR 68.1 follows this trend.

Several modifications of the simple Unified Model for radio galaxies and quasars, involving the effects of absorption towards the central source, the radio core, the scatterers and the NLR, are suggested in the case of 3CR 68.1: (i) even for highly inclined AGNs like the radio galaxies, the radio core dominance is among the smallest ($\log R = -3.2$). In the lower inclination case, a possibility is that the reddened line-of-sight combined with the very weak radio core is the result of radio free-free absorption by dusty, ionized gas. This could be tested by determining the shape of the radio spectrum, and also by searching for X-ray absorption edges of O VII and O VIII (as for IRAS 13349+2438 – Beichman et al. 1986; Brandt et al. 1997; see also Leighly et al. 1997; Grupe et al. 1997). (ii) the polarization position angle is not perpendicular to the radio jets as discussed above, suggesting a partially filled or partially obscured cone, and (iii) the narrow-line (NLR) equivalent widths are similar to those in our mean unreddened quasar spectrum, and also similar to the composite lobe-dominated quasar spectrum of Baker & Hunstead (1995) formed from the

Molonglo sample. If 3CR 68.1 were reddened by the amounts implied by our modeling, then the continuum is suppressed by 20 to 30 times. If the low-ionization NLR extends well beyond the dusty torus, the NLR should suffer much less reddening and EW(NLR) should be enhanced by 20 to 30 times. The reddening of the NLR in the Hill et al. radio-galaxies, the reddened scattered spectrum of 3C 68.1, and a partially obscured cone, all suggest significant absorption.

We reach a limit to this simple interpretation if there is significant forward-scattered, less-polarized light; in this case the obscuration we derive from the steepening of the UV-optical spectrum would be an underestimate. But then the geometry of the simple Unified Scheme breaks down. In this regard, 3CR 68.1 makes an especially interesting and important comparison with the (only) other scattered-light, luminous radio-loud quasar OI 287. In OI 287 the scattered light is thought to be scattered by electrons in the outer regions of a geometrically thin, dusty disk that obscures the center completely at UV-optical wavelengths. This explains its polarization parallel to the radio jets. 3CR 68.1 also shows polarization that is not exactly perpendicular to the radio jets; a polarized component as in OI 287 provides an alternative explanation to a partially filled or partially obscured scattering cone.

Overall 3CR 68.1 fits well into the Unified Scheme, although it falls short of being a textbook example in several potentially interesting respects. These 'shortcomings' may in the future provide opportunities to probe intrinsic obscuring structures common to all quasars.

5. Summary

We have presented optical spectropolarimetry of 3CR 68.1, a quasar with an unusual combination of extreme optical, radio, and polarization properties. The polarization increases from ≈5% at λ_{rest} = 4000Å, to >10% at λ_{rest} = 2000Å, with a nearly constant position angle of ≈ 53°. Broad-emission lines are polarized the same as the continuum. We have measured parameters of the emission lines and absorption lines in the total light spectrum.

We have argued that scattering by dust or electrons is the polarization mechanism, and that we see the quasar along two reddened lines of sight. We have modeled this situation and compared our models with published photometry. The implied reddenings are modest, $A_V = 0.7$ for the scattered line of sight, and $A_V = 1.1$ to 1.6 for the direct line of sight, depending on the intrinsic polarization of the scattered light and the possible contribution of light from an elliptical host galaxy implied by Ca II K absorption.

We have interpreted the geometry in terms of unified models such that 3CR 68.1 is observed at a line of sight skimming the edge of an obscuring torus. While this interpretation appears correct and explains the main properties 3CR 68.1 very well, a few interesting issues remain in the details of the geometry and in the placement and nature of both the scattering and absorbing material.

We thank Ron Quick, Randy Campbell, Tom Bida, and Bob Goodrich for their assistance during our Keck run, Hien Tran for useful discussions, Mark Dickinson for providing some IRAF scripts, and Derek Wills for measuring the interstellar polarization toward 3CR 68.1. We thank the editor and the referee, Dean Hines, whose suggestions improved the paper. BJW gratefully acknowledges support through NASA LTSA grant number NAG5-3431. The W. M. Keck Observatory is a scientific partnership between the University of California and the California Institute of Technology, made possible by the generous gift of the W. M. Keck Foundation. This research has made use of the NASA/IPAC Extragalactic Database (NED) which is operated by the Jet Propulsion Laboratory, California Institute of Technology, under contract with

the National Aeronautics and Space Administration. Work performed at the Lawrence Livermore National Laboratory is supported by the DOE under contract W7405-ENG-48.

REFERENCES

Aldcroft, T. L., Bechtold, J. & Elvis, M. 1994, ApJS, 93, 1

Aldcroft, T. L., Elvis, M., & Bechtold, J. 1993, AJ, 105, 2054

Antonucci, R. R. J. 1993, ARAA, 31, 473

Antonucci, R. R. J., Kinney, A. L., & Hurt, T. 1993, ApJ, 414, 506

Antonucci, R. R. J., & Ulvestad, J. S. 1988, ApJ, 328, 569

Baker, J. C., & Hunstead, R. W. 1995, ApJ, 452, 95L

Barthel, P. D. 1989, ApJ, 336, 606

Beichman, C. A., Soifer, B. T., Helou, G., Chester, T. J., Neugebauer, G., Gillett, F. C., Low, F. J. 1986, ApJ, 308, L1

Boksenberg, A., Carswell, R. F., & Oke, J. B. 1976, ApJ, 206, L121

Brandt, W. N., Mathur, S., Reynolds, C. S., Elvis

Bregman, J. N., Glassgold, A. E., Huggins, P. J., Kinney, A. L. 1985, ApJ, 291, 505

Bridle, A. H., Hough, D. H., Lonsdale, C. J., Burns, J. O., & Laing, R. A. 1994, AJ, 108, 766

Brotherton, M. S., Tran, H. D., van Breugel, W., Dey, A., & Antonucci, R. R. J. 1997, ApJ, 487, L113

Brown, J. C., & McLean, I. S. 1977, A&A, 57, 141

Burstein, D., & Heiles, C. 1982, AJ, 87, 1165

Cardelli, J. A., Clayton, G. C., & Mathis, J. S. 1989, ApJ, 345, 245

Cimatti, A., Dey, A., van Breugel, W., Antonucci, R., & Spinrad, H. 1996, ApJ, 465, 145

Cohen, M. H., Vermeulen, R. C., Ogle, P. M., Tran, H. D., & Goodrich, R. W. 1997, ApJ, 484, 193

Cohen, M. H., et al. 1995, ApJ, 448, L77

Courbin, F., Hutsemekers, D., Meylan, G., Magain, P., & Djorgovski, S. G. 1997, A&A, 317, 656

De Breuck, C., Brotherton, M. S., Tran, H. D., van Breugel, W., & Röttgering, H. 1998, AJ, submitted

Dey, A., & Spinrad, H. 1996, ApJ, 459, 133

Elvis, M., et al. 1994, ApJS, 95, 1

Goodrich, R. W., Cohen, M. H., & Putney, A. 1995, PASP, 107, 179

Goodrich, R. W., & Miller, J. S. 1988, ApJ, 331, 332

Goodrich, R. W., & Miller, J. S. 1995, ApJ, 448, L73

Grupe, D., Wills, B. J., Wills, D., & Beuermann, K. 1997, A&A, in press

Hill, G. J., Goodrich, R. W., & DePoy, D. L. 1996, ApJ, 462, 163

Hines, D. C., & Wills, B. J. 1995, ApJ, 448, L69

Hines, D. C., & Wills, B. J. 1993, ApJ, 415, 82

Hoekstra, H., Barthel, P.D., & Hes, R. 1997, A&A, 319, 757

Kinney, A.L., Calzetti, D., Bohlin, R.C., McQuade, K., Storchi-Bergmann, T. & Schmitt, H.R. 1996, ApJ, 467, 38

Laing, R. A., Riley, J. M., Longair, M. S. 1983, MNRAS, 204, 151

Leahy, J. P., Muxlow, T. W. B., & Stephens, P. W. 1989, MNRAS, 239, 401

Ledden, J. E., & Odell, S. L. 1985, ApJ, 298, 630

Leighly, K. M., Kay, L. E., Wills, B. J., Wills, D., & Grupe, D. 1997, ApJL, in press

Longair, M., & Gunn, J. 1975, MNRAS, 170, 121

Massey, P., & Gronwall, C. 1990, ApJ 358, 344

Massey, P., Strobel, K., Barnes, J. V., & Anderson, E. 1988, ApJ, 328, 315

Miller, J. S., Robinson, L. B., & Goodrich, R. W. 1988, in Instrumentation for Ground-Based Optical Astronomy, ed. L. B. Robinson, (New York: Springer-Verlag), 157

Miller, J. S., 1997, in Mass Ejection from Active Galactic Nuclei, ASP Conference Series, 128, 69

Miller, J. S., & Antonucci, R. R. J. 1985, ApJ, 297, 621

Moore, R. L., & Stockman, H. S. 1981, ApJ, 243, 60

Moore, R. L., & Stockman, H. S. 1984, ApJ, 279, 465

Neugebauer, G., Oke, J. B., Becklin, E. E., & Matthews, K. 1979, ApJ, 230, 79

Ogle, P. M., et al. 1997, ApJ, 482 , L37

Ogle, P. M. 1997, in Mass Ejection from Active Galactic Nuclei, ASP Conference Series, 128, 78

Oke, J. B., et al. 1995, PASP, 107, 375

Orr, M. J. L., & Browne, I. W. A. 1982, MNRAS, 200, 1067

Prevot, M. L., Lequeux, J., Prevot, L., Maurice, E., & Rocca-Volmerange, B. 1984, A&A, 132, 389

Rieke, G. H., Wisniewski, W. Z., & Lebofsky, M. J. 1982, ApJ, 263, 73

Rudy, R. J., & Schmidt, G. D. 1988, ApJ, 331, 325

Schmidt, G. D., Elston, R., & Lupie, O. L. 1992, AJ, 104, 1563

Schmidt, G. D., Hines, D. H., & Smith, P. S. 1997, in Mass Ejection from Active Galactic Nuclei, ASP Conference Series, 128, 106

Smith, H. E., & Spinrad, H. 1980, ApJ, 236, 419

Sprayberry, D., & Foltz, C. B. 1992, ApJ, 390, 39

Stein, W. A., & Sitko, M. L. 1984, AJ, 89, 1688

Tran, H. D., Cohen, M. H., Goodrich, R. W., & di Serego Alighieri, S. 1998, ApJ, in press

Voges, W., et al. 1996, IAU Circ., 6420, 2 (http://www.rosat.mpe-garching.mpg.de/survey/rass-bsc/)

Webster, R. L., Francis, P. J., Peterson, B. A., Drinkwater, M. J., & Masci, F. J. 1995, Nature, 375, 469

Wills, B.J., & Brotherton, M. S. 1995, ApJ, 448, 81L

Wills, B.J., & Hines, D. C. 1997, in Mass Ejection from Active Galactic Nuclei, ASP Conference Series, 128, 99

Wills, B. J., Wills, D., Evans, N. J., II, Natta, A., Thompson, K. L., Breger, M., & Sitko, M. L, 1992, ApJ, 400, 96

Wills, B. J., Thompson, K. L., Han, M., Brotherton, M. S., Netzer, H., Baldwin, J. A., Wills, D., Ferland, G. J., & Browne, I. W. A. 1995, ApJ, 447, 139

Witt, A., Thronson, H. A., Jr., & Capuano, J. M., Jr. 1992 ApJ, 393, 611

Table 1. Emission-Line Measurements

Line Identification	Center[a] (Å)	Obsrved Flux ($10^{-16} ergs\ s^{-1}\ cm^{-2}$)	EW[b] (Å)	FWHM[c] ($km\ s^{-1}$)	Galactic Factor[d] ($A_V = 0.15$)
Total C III] λ1909	4251.0±0.4	7.0±1.0	19.7±1.8	1300±200	1.45
Broad C III] λ1909	4249±3	5.9±0.8	13±1.8	7400±800	1.45
Narrow C III] λ1909	4251.0±0.4	3.0±0.1	6.7±2.2	800±50	1.45
C II] λ2326	5183.5±1.0	1.1±0.4	1.1±0.4	1300±400	1.44
[Ne IV] λ2425	5399.5±0.4	1.6±0.1	1.3±0.1	700±50	1.39
Total Mg II λ2800 [e]	6226±2	40±8	28±5	4500±500	1.30
Broad Mg II λ2800	6227±5	38±5	25±2	14400±500	1.30
Narrow Mg II λ2800	6226±2	5.5±0.5	3.1±0.3	2000±200	1.30
He I λ2830	6314.2±0.8	1.4±0.5	0.8±0.3	1100±200	1.30
O III λ3133	6978±2	1.2±0.4	0.7±0.2	1400±200	1.27
He II λ3203 (+ Fe II?)	7139±1.5	1.5±0.3	7.9±1.6	1600±200	1.27
[Ne V] λ3346	7452.6±0.3	1.3±0.4	0.8±0.2	700±100	1.25
[Ne V] λ3426 + O III λ3444[f]	...	...	...	...	...
[O II] λ3727	8309.0±0.3	6.8±0.4	3.5±0.2	500±40	1.24
[Ne III] λ3869 + H8 + He I λ3868	8623.3±0.3	6.8±1.0	3.5±0.6	600±70	1.23
[Ne III] λ3967 + Hϵ[g]	...	...	...	...	...

[a]Air wavelengths.

[b]Corrected to rest-frame.

[c]Corrected for the instrumental resolution of ∼10Å.

[d]Flux densities should be multiplied by this factor to correct for Galactic reddening.

[e]The absorption lines and He I λ2830 were interpolated across in order to estimate the integrated flux and equivalent width for Mg II. The emission line peak was estimated based on the unabsorbed narrow component wings.

[f]The [Ne V] λ3426 + O III λ3444 blend, often easily measured in good spectra of quasars and radio galaxies, falls at the same wavelength as atmospheric A band absorption (which we were unable to remove well with our standard star).

[g]The [Ne III] λ3967 + Hϵ blend is coincident with Ca II H absorption, and also with a strong night sky feature. This blend cannot be reliably measured.

Table 2. Absorption-Line Measurements[a]

Identification	Center[b] (Å)	λ_{rest} (Å)	z_{abs}	EW[c] (Å)
Fe II λ2382	5301.7±0.7	2382.0	1.2257(3)	1.0±0.3
Fe II λ2586	5757.3±0.1	2585.9	1.2264(1)	1.0±0.2
Fe II λ2600	5785.5±0.1	2599.4	1.2257(1)	2.0±0.2
Mg II λ2796	6221.0±0.5	2795.5	1.2254(2)	6.5±0.2
Mg II λ2803	6238.3±0.2	2802.7	1.2258(1)	4.4±0.2
Mg I λ2853	6348.3±0.6	2852.1	1.2258(2)	1.1±0.2
He I λ3187.7?	7093.0±1.0	3187.7	1.2251(3)	1.5±0.4
Ca II K	8767.0±0.5	3933.7	1.2287(1)	5.0±0.8

[a]Uncertanties quoted denote the range of acceptable measurements rather than formal 1 σ fitting errors.

[b]Air wavelengths.

[c]Equivalent widths (EWs) are in the observed frame.

Table 3. Model Parameters

Model	P_s	Galaxy	Direct A_V	Scattered/Direct
A	80%	No	1.2	0.04
B	50%	No	1.3	0.06
C	20%	No	1.6	0.13
A_G	80%	Yes	1.1	0.06
B_G	50%	Yes	1.2	0.09
C_G	20%	Yes	1.5	0.17

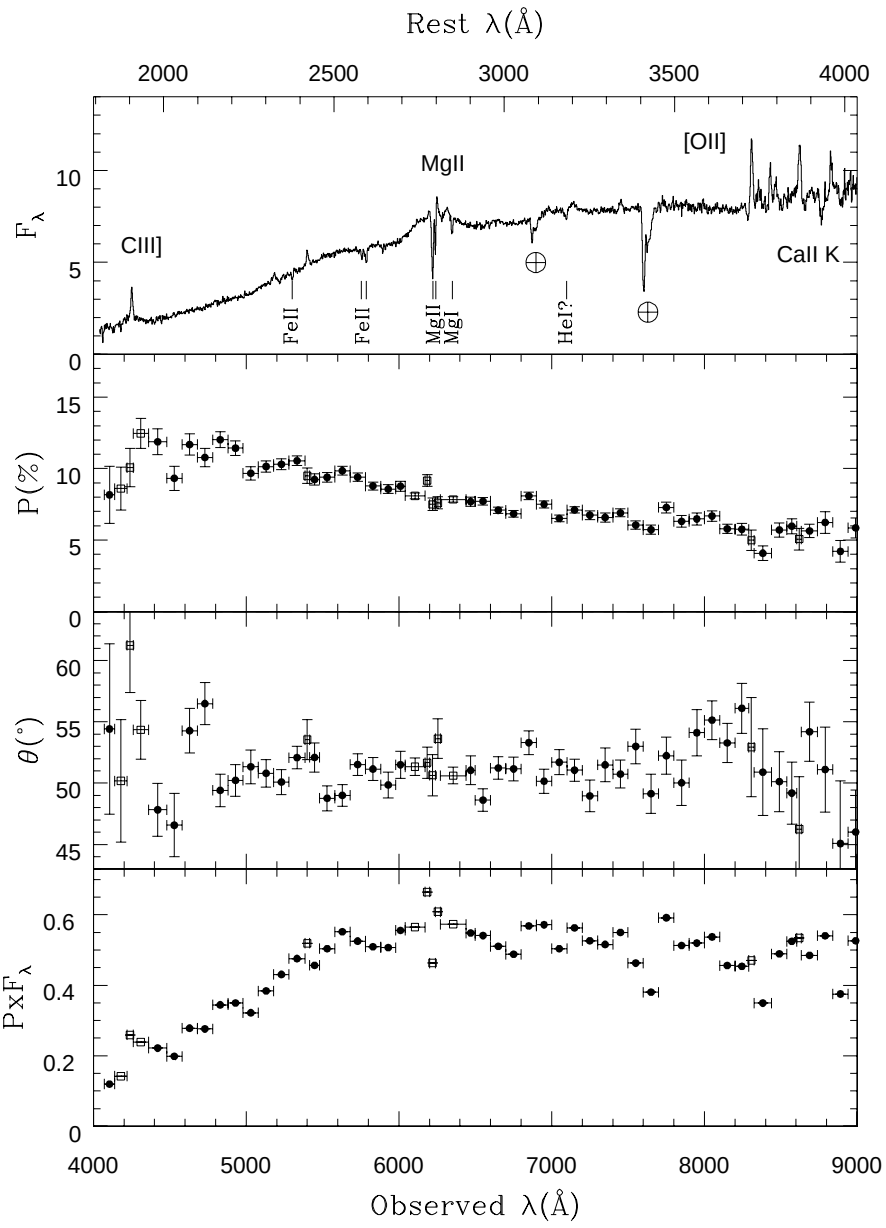

Fig. 1.— Spectropolarimetric results for 3CR 68.1. The top abscissa shows rest-frame wavelengths, while the bottom abscissa shows observed-frame wavelengths, both in Å. The top panel is the total flux spectrum (in 10^{-17} ergs s^{-1} cm^{-2} Å^{-1}), with some prominent features labeled and narrow absorption lines marked from below. The second panel from the top shows the percentage polarization. The third panel is the polarization position angle in degrees. The bottom panel shows the polarized flux, the product of the binned fractional polarization and binned total light spectrum. Vertical error bars are 1 σ, while the horizontal bars show the extent of the bins as described in the text.

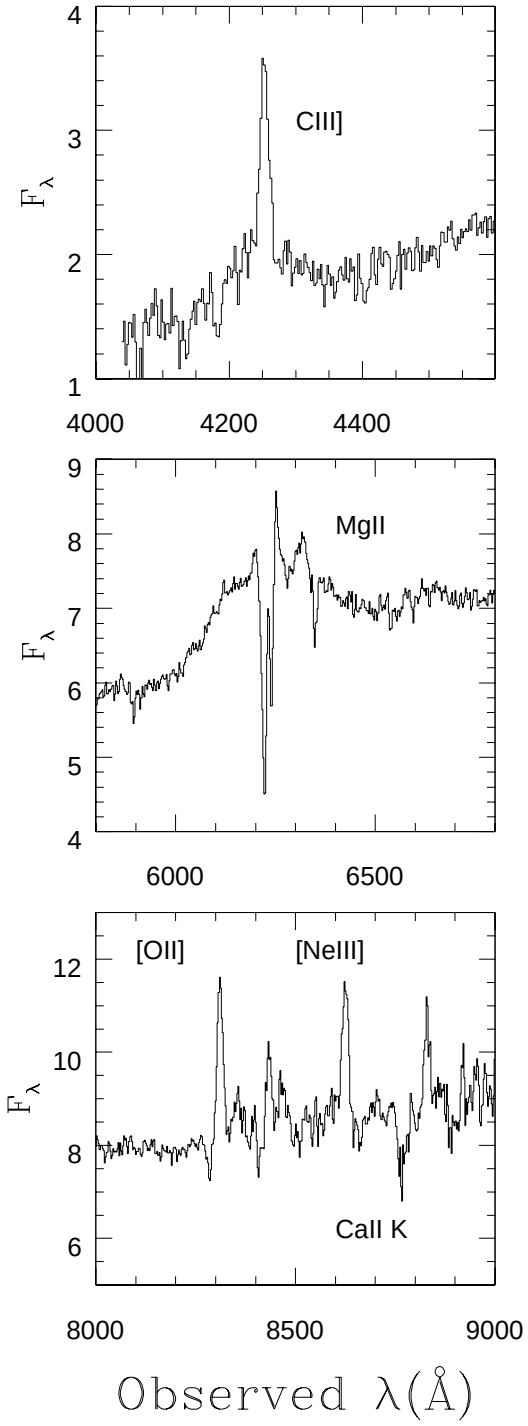

Fig. 2.— Detail of several regions of the total light spectrum. Wavelengths are observed frame, while flux units are 10^{-17} ergs s^{-1} cm^{-2} $Å^{-1}$.

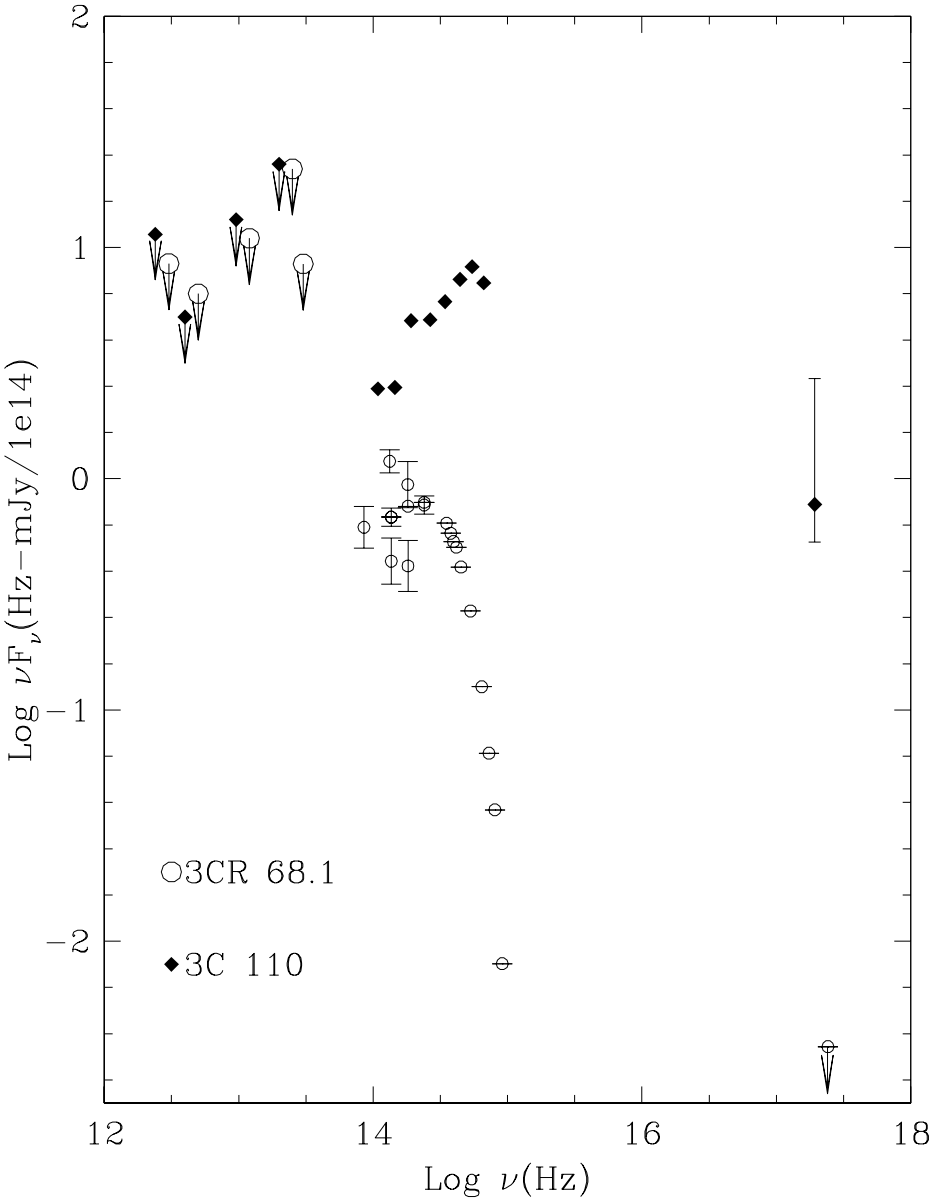

Fig. 3.— The (observed-frame) spectral energy distribution for 3CR 68.1. The optical points are from Neugebauer et al. (1979) and Smith & Spinrad (1980). Mid and near-IR points are from Neugebauer et al. (1979), Stein & Sitko (1984), and Rieke et al. (1982). The X-ray upper limit comes from the RASS survey limit, after checking the count rates and standard deviations in the 3CR 68.1 region of sky, and using standard flux-density conversions, assuming $F_\nu \propto \nu^{-2.25}$ and a Galactic hydrogen column density $N_H = 6 \times 10^{20}\,\mathrm{cm}^{-2}$ (Voges et al. 1996). The data for 3C 110, shifted to the observed frame of 3CR 68.1, comes from the Atlas of Elvis et al. (1994), with the near-IR and optical data for only the October 1984 epoch plotted.

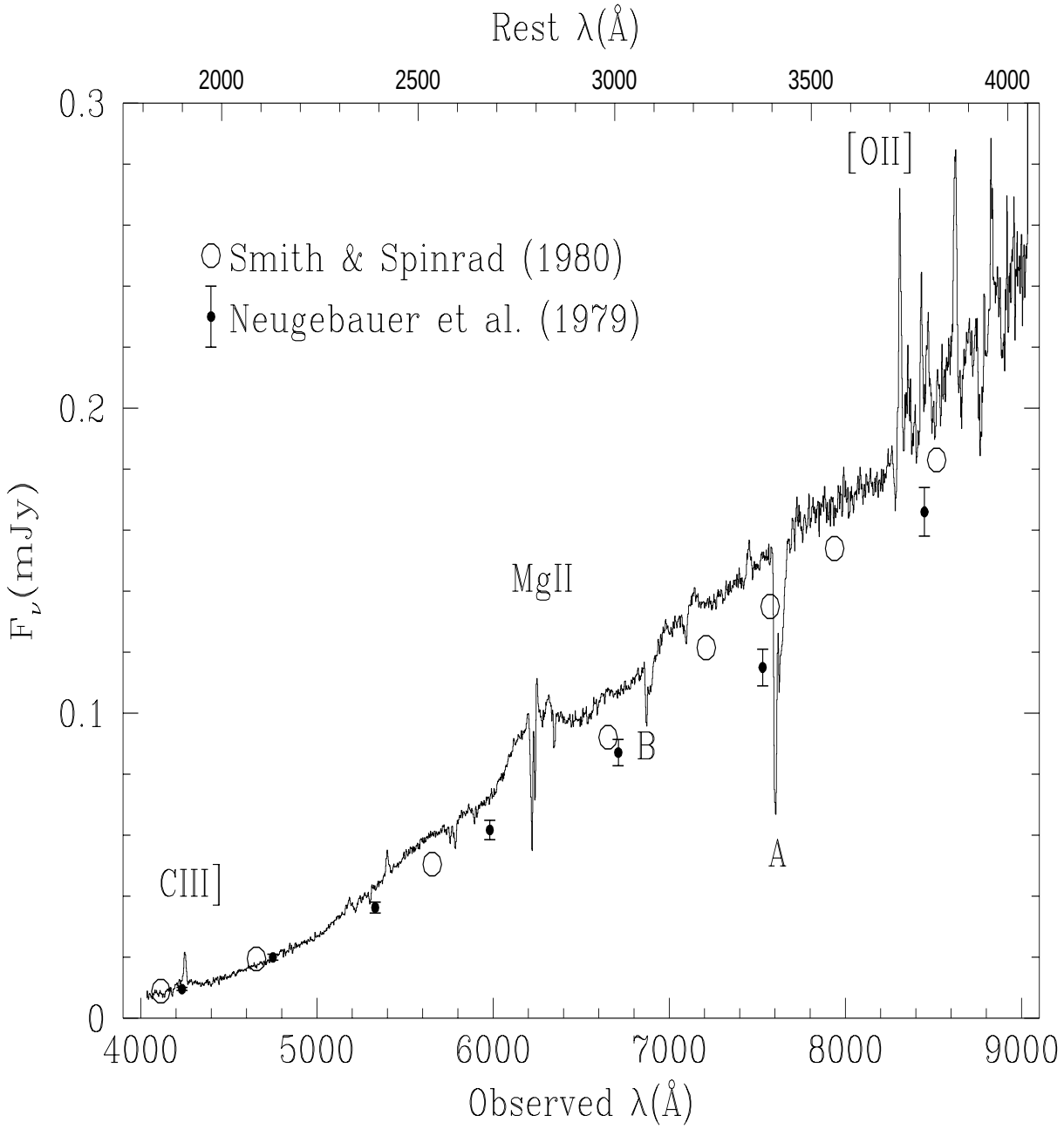

Fig. 4.— Comparison our total flux density spectrum with those of Neugebauer et al. 1979 (*dark circles*, error bars as given by Neugebauer et al. 1979) and Smith & Spinrad 1980 (*open circles*).

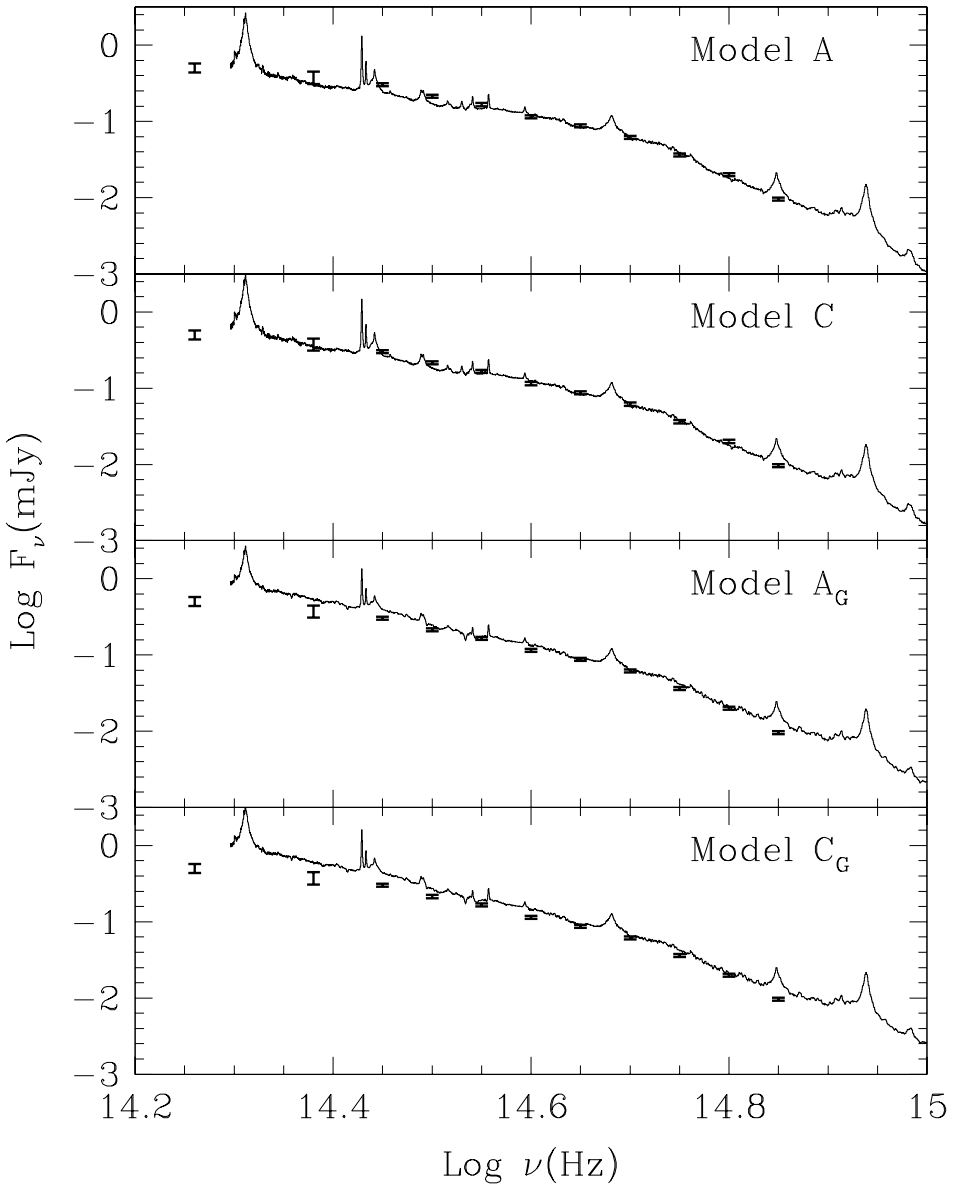

Fig. 5.— The extreme models from Table 3 and the text, with and without a host galaxy component, compared with the Neugebauer et al. (1979) 3CR 68.1 photometry, B to H. The bold errors bars are as given by Neugebauer et al.

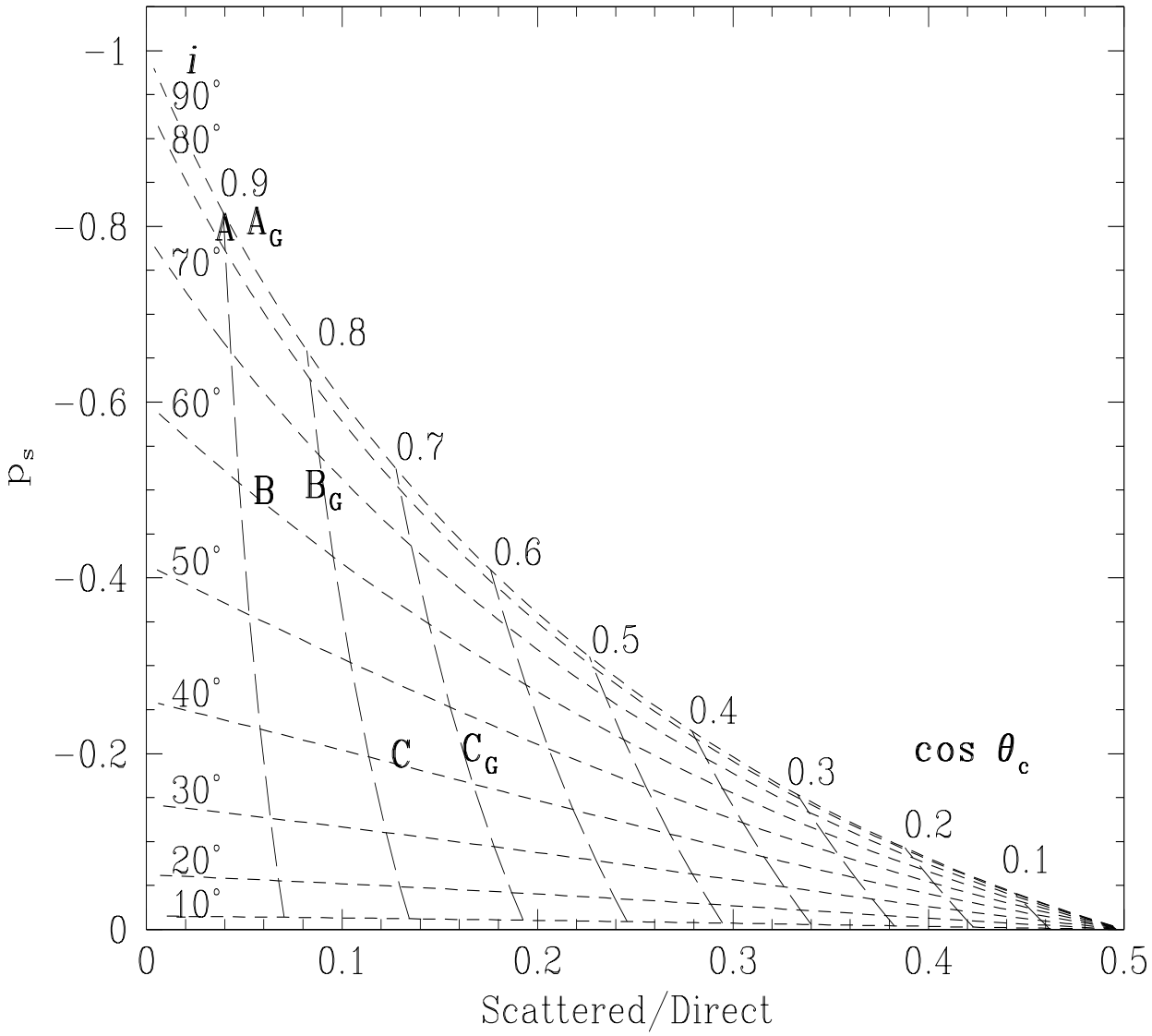

Fig. 6.— A simple scattering model. The fractional linear polarization of scattered light (p_s) is plotted against the ratio of scattered to direct light for a uniformly filled cone of wavelength-independent scatters. The model includes no reddening or obscuration. The negative sign on p_s indicates that the electric vector of the polarized light is perpendicular to the cone axis. Model lines show the effects of varying i, the inclination of the axis to the line of sight, and the cosine of the half opening angle of the cone, θ_c. Models A, B, and C correspond to our data on 3CR 68.1 under the assumptions that the host galaxy light is negligible and p_s = 80%, 50%, and 20%, respectively. The G subscripts are for models with a host galaxy contribution.